ACS ENGINEERING Au
AN OPEN ACCESS JOURNAL OF THE AMERICAN CHEMICAL SOCIETY

pubs.acs.org/engineeringau
Article

Combined Effects of Salt and Microplastics on Evaporation and Crystallization Dynamics in Porous Media

Sahar Jannesarahmadi,* Milad Aminzadeh,* Birte Hindenlang, Berit Zeller-Plumhoff, Fabian Wilde, Mehdi Mahdaviara, Patrick Huber, and Nima Shokri*

Cite This: https://doi.org/10.1021/acsengineeringau.5c00118
Read Online

ACCESS | Metrics & More | Article Recommendations

ABSTRACT: This study investigates the combined effects of salinity and microplastic contamination on the evaporation process and salt crystallization in porous media through complementary column- and pore-scale experiments. Laboratory soil columns were packed with either pure sand or sand mixed with 5% (w/w) poly(vinyl chloride) (PVC) microplastics and subsequently saturated with freshwater or saline (NaCl) solution. Evaporation and crystallization dynamics were monitored by using mass loss measurements, surface optical and thermal imaging, and synchrotron X-ray tomography. Results show that salinity consistently suppressed evaporation by roughly 25−30%, whereas PVC microplastics enhanced it, generating substantial differences in cumulative water loss across treatments. Moreover, thermal imaging revealed distinct surface responses: NaCl samples developed salt crusts that progressively reduced local temperature contrasts and led to more spatially uniform surface conditions, whereas PVC-NaCl samples exhibited lower mean surface temperatures but substantially higher spatial variability, reflected in larger and more persistent temperature anomalies during drying. Pore-scale μCT imaging further confirmed that microplastics altered crystallization patterns by redistributing salt deposition over the upper part of the sand profile and modifying the nucleation behavior. Together, these findings underscore the complex interplay between microplastics and salinity, with implications for soil moisture regulation, surface energy flux, and environmental monitoring strategies.

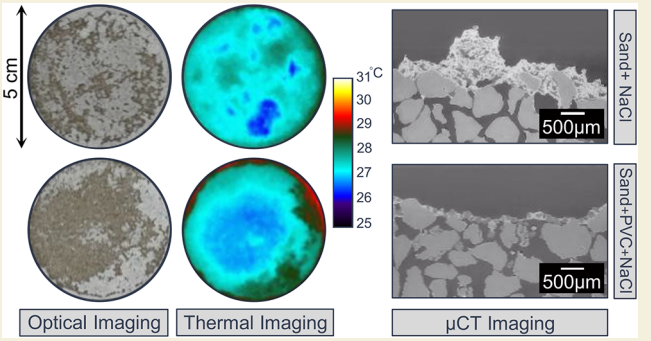

KEYWORDS: *porous media, evaporation, salt crystallization, microplastics, surface temperature, X-ray tomography*

1. INTRODUCTION

Evaporation from porous media is a fundamental process in natural environments and engineering applications, influencing a wide range of phenomena from soil moisture dynamics and land−atmosphere interactions to durability of building materials.[1−5] In the presence of dissolved salts, this process becomes more complex. As evaporation proceeds, the concentration of dissolved ions near the vaporization plane increases until it exceeds the solubility limit, initiating nucleation and leading to the formation and accumulation of salt crystals at or near the surface.[6,7] These crystals modify the pore structure and disrupt capillary-driven flow, thereby influencing evaporation rates, surface energy fluxes, and surface morphology. Such processes have significant implications for soil health and broader engineering challenges in saline-affected regions.[8−11] The extent of these impacts is closely linked to the morphology and hydraulic connectivity of the resulting salt crust. Porous and hydraulically connected efflorescence can enhance evaporation by sustaining capillary flow, whereas dense, detached crusts may suppress it by creating a diffusive barrier.[12−16] Recent experimental and theoretical studies further demonstrate that salt precipitation and subsurface convection can couple surface crust formation with fluid transport in the underlying porous medium, generating spatially variable salt fluxes and modifying evaporation and heat exchange across saline landscapes.[17−19]

While numerous studies have examined saline water evaporation from porous media and associated crystallization dynamics,[20−23] the potential influence of microplastics (MPs) on these processes has received limited attention. Microplastics as emerging environmental contaminants enter the soil from various sources, ranging from plastic mulching and wastewater irrigation to sludge-based fertilization, thus affecting soil

Received: December 18, 2025
Revised: March 1, 2026
Accepted: March 2, 2026

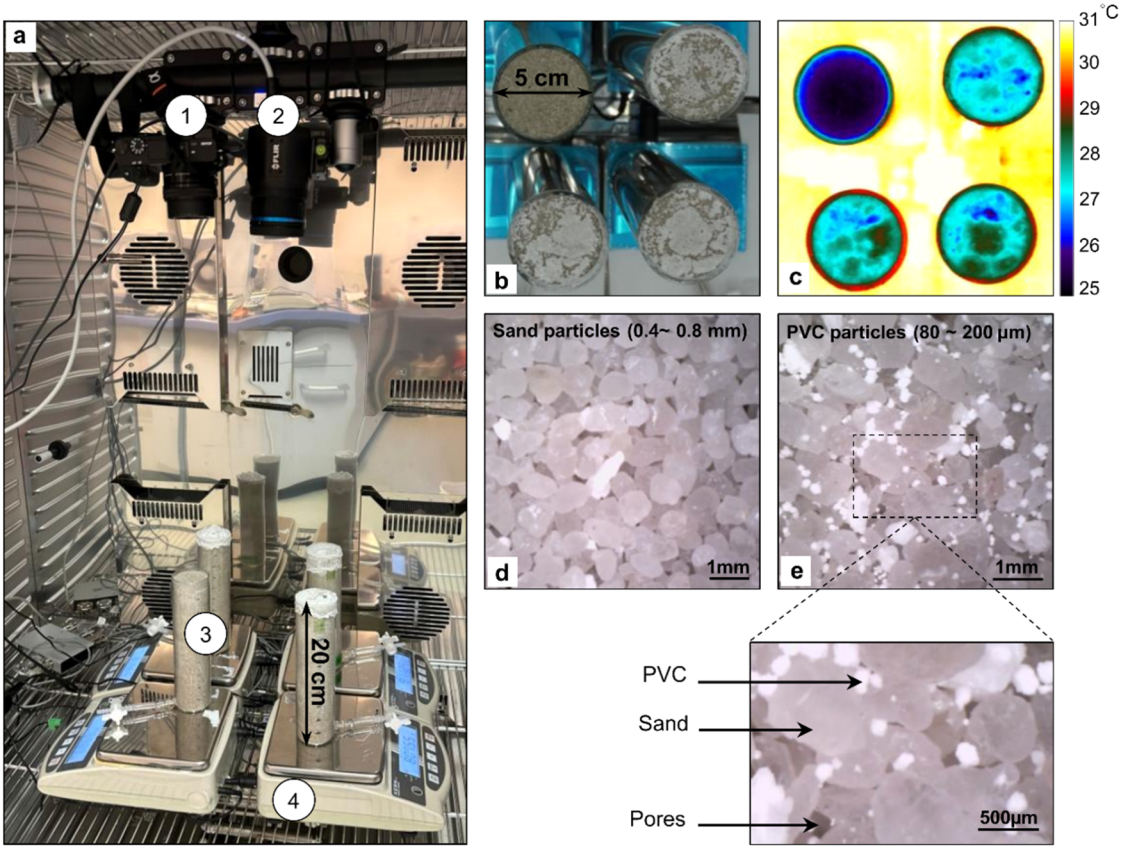

Figure 1. (a) Experimental setup in a climate chamber with controlled temperature and humidity. The setup components include (1) an optical camera, (2) an IR camera, (3) sample columns, and (4) balances. Surface of samples saturated with 5% NaCl solution, and the reference sample saturated with freshwater captured by (b) an optical camera and (c) an IR camera. Microscopic images from the surface of (d) pure sand and (e) sand containing 5% PVC.

properties and processes.[24−32] Microplastics possess distinct properties, such as high specific surface area, low density, and hydrophobicity, which can significantly influence soil physical and chemical characteristics. Depending on their size, shape, and surface characteristics, microplastics can alter soil texture, modify pore geometry, and disrupt flow continuity by either obstructing or enhancing capillary pathways, thus impacting key transport properties, evaporation, and subsurface flow processes.[33−35] Previous studies indicate that microplastic accumulation alters soil hydraulic conductivity, water-retention behavior, and pore-size distribution, thus influencing water flow, infiltration, and moisture distribution across different soil textures.[36−38]

Considerable research has addressed the individual effects of salinity and microplastics on a wide range of processes in porous media; however, their interactive influence on evaporation dynamics, salt crystallization, and the resulting surface thermal signatures remains less understood. In this study, we systematically investigate the coupled effects of microplastics and salinity on the evaporation and salt crystallization in porous media. Integrating column-scale drying experiments with pore-scale observations, we quantify their impacts on evaporative mass loss, crystallization patterns, and surface temperature variations. Our results provide new mechanistic insights into microplastic-salt interactions and their implications for soil water balance and soil health considerations.

2. MATERIALS AND METHODS

2.1. Laboratory Column Experiments

To investigate the combined effects of microplastics and salinity on evaporation dynamics and surface temperature variation, a series of laboratory experiments was conducted under controlled ambient conditions in a climate chamber (Memmert, HPP750eco) maintained at a relative humidity of 30% and an air temperature of 30 °C (Figure 1).

Glass cylindrical columns (5 cm internal diameter and 20 cm height) were packed with sand characterized by particle sizes ranging from 0.4 to 0.8 mm (see Jannesarahmadi et al., 2023 for more details). Poly(vinyl chloride) (PVC), one of the most prevalent types of microplastics in terrestrial environments, was selected and thoroughly mixed with dry sand at a concentration of 5% by mass, which lies within the range of microplastic contents reported for contaminated soils in industrial environments (0.03−6.7% by mass[36−39]). The PVC particles ranged in size from 80 to 200 μm with a density of 1.4 g/cm^3. Sodium chloride (NaCl) solutions with concentrations of 5% by mass were prepared for sample saturation. Salinity in the column experiments was fixed at 5% NaCl to ensure observable crystallization within the experimental time frame. While salinity levels under natural environmental conditions may alter the onset and extent of salt precipitation, the primary mechanisms identified here are expected to remain valid. Nevertheless, the magnitude and timing of crystallization may vary under different salinity conditions.

To isolate and compare the effects of salinity and microplastics, we conducted our experiments on: (i) pure sand saturated with 5% NaCl solution, (ii) sand mixed with 5% PVC and saturated with freshwater, and (iii) sand mixed with 5% PVC and saturated with 5% NaCl solution. Each condition was tested in a dedicated experimental phase.

https://doi.org/10.1021/acsengineeringau.5c00118
ACS Eng. Au XXXX, XXX, XXX−XXX

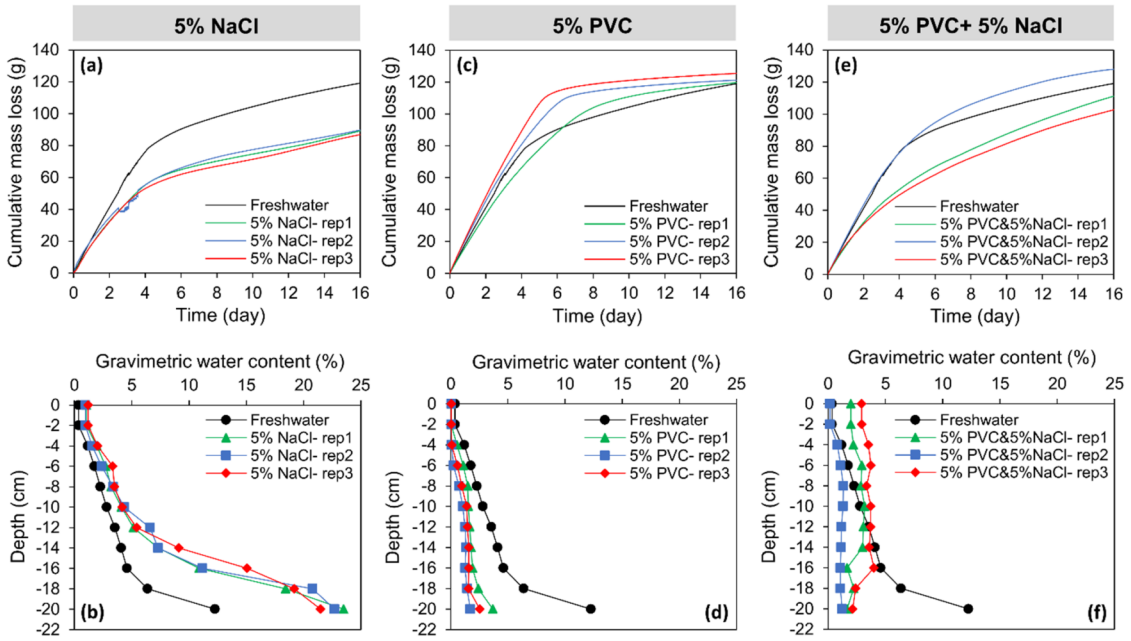

Figure 2. Cumulative water mass loss versus time (a, c, e), and corresponding gravimetric water content profiles versus depth (b, d, f) for the tested samples (measured at the end of evaporation experiments). The legend denotes the treatments: samples saturated with 5% NaCl, samples containing 5% PVC, and samples containing 5% PVC saturated with 5% NaCl solution, with the freshwater sample serving as the reference.

Within each set, three identical columns were prepared to ensure the reproducibility of the results. Additionally, a column consisting of pure sand saturated with freshwater was included as a reference in all experimental sets. The columns were fully saturated only once at the beginning of the experiment, and evaporative water loss was continuously recorded at 10 min intervals using digital balances (Kern EW 6200−2NM), with a repeatability of 0.01 g and a linearity of 0.03 g. An infrared imager (FLIR A700 PRO-F) and a digital camera (SONY α 6400) were used to simultaneously capture the surfaces of columns every 10 min. The optical images were used to monitor the evolution of surface crystals, while thermal images (640 × 480 pixels) provided spatially resolved surface temperature with an approximate resolution of 0.25 mm/pixel. A MATLAB code was developed to process thermal images and extract the temperature details.

2.2. Pore-Scale Visualization Using X-ray Microtomography

Pore-scale experiments were operated at the DESY PETRA III synchrotron facility (Hamburg, Germany) to gain insights into the impact of microplastics on crystallization dynamics and thus complement column-scale observations. The experiment focused on two selected cases: (i) pure sand saturated with 25% NaCl solution and (ii) sand mixed with 5% PVC by mass and saturated with 25% NaCl solution. The salt concentration was intentionally set at 25% in both cases to accelerate crystallization within the limited beamline access time. The resulting μCT observations therefore aim to resolve the spatial localization of salt precipitation within the near-surface pore network, which is governed primarily by pore geometry and capillary transport rather than the exact salinity used in the column-scale experiments. Acrylic cylindrical columns (10 mm height and 7 mm diameter) were selected to fit within the field of view of the imaging setup and were filled with sand and microplastic particles. Pore-scale imaging was then performed using X-ray microcomputed tomography (μCT) to visualize the 3D pore structure, the crystallization dynamics, and the spatial distribution of salt and microplastics in porous media after the drying process. The scans were acquired at a photon energy of 2 keV with an exposure time of 170 ms over 2500 projections per sample, yielding a voxel size of 2.58 μm after 2× binning. Beam energy and imaging parameters were adjusted to optimize the contrast between sand grains, salt crystals, and microplastics.

2.3. Image Processing and Data Segmentation

The acquired projections were preprocessed by flat and dark field correction, pixel filtering, and beam current normalization. Afterward, the projections were tomographically reconstructed by filtered backprojection (FBP) using the tomographic reconstruction pipeline, implemented in IDL and MATLAB and the ASTRA toolbox (R2024b, The MathWorks, Inc., USA).[40−42]

The reconstructed tomograms were further processed by iterative nonlocal means filtering using two iterations to reduce the existing noise while retaining the occurring features in the samples.[43] To remove artifacts at the border of the sample volume, the filtered tomograms were masked to the relevant volume using FIJI.[44] All subsequent processing and segmentation were conducted in Avizo (Avizo 2021.1, FEI SAS, Thermo Scientific, France). In the processing step, the different height steps of the same sample were stitched into one sample by registering them with each other. Ultimately, the segmentation of the sand, water, microplastic, and salt crust was performed in separate steps. First, the background was removed by masking the tomograms with threshold segmentation of the relevant regions. Afterward, the infiltrated scan was segmented based on water and sand by region growing. The sand segmentation was registered on the dried scan and masked from the tomograms. By this, sand was removed from the tomograms, and the segmentation of the salt crust was improved.

The sample containing microplastics was segmented similarly. However, the microplastic could not be segmented in the infiltrated state due to an overall low contrast between the features. In the infiltrated state, it exhibited an attenuation coefficient similar to that of water and was therefore not completely visible. In the dried scan, a similar problem occurred, since the microplastic had a similar gray scale to the sand. Therefore, the sand and microplastics were segmented in one mask and subsequently differentiated by their specific sizes (400−800 μm for sand and 80−200 μm for PVC). Nevertheless, a complete differentiation between sand and microplastic was not possible, so only a qualitative overview of the microplastic distribution can be given. From the obtained segmentations, the height distributions of the different components in the sample were calculated by using MATLAB.

https://doi.org/10.1021/acsengineeringau.5c00118
ACS Eng. Au XXXX, XXX, XXX−XXX

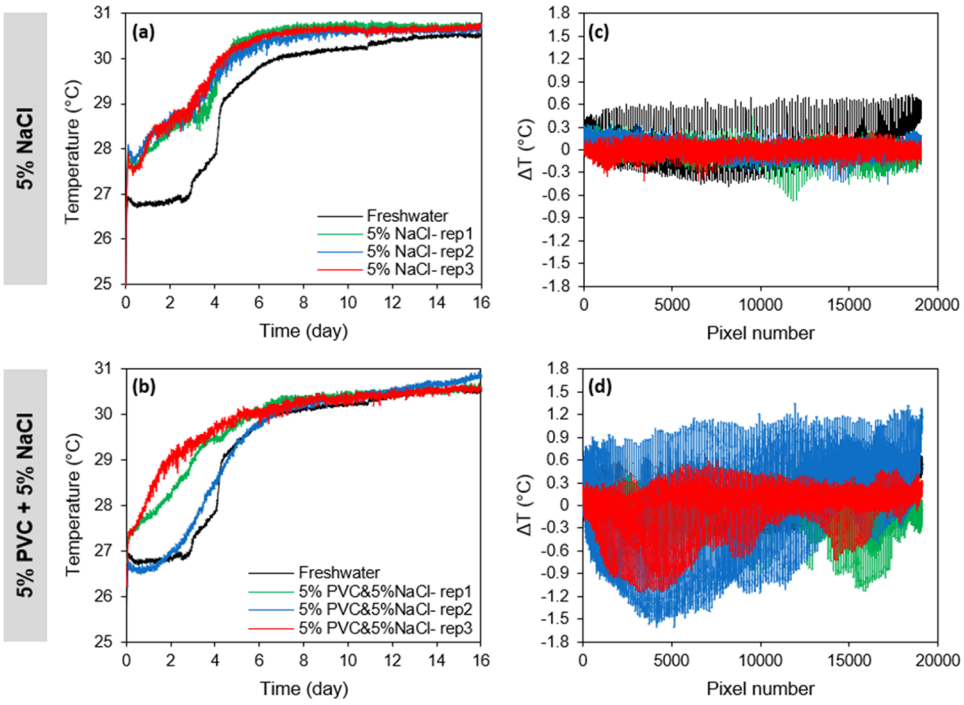

Figure 3. (a, b) Temporal evolution of the mean surface temperature. (c, d) Variation of surface temperature anomalies (ΔT, defined as individual pixel temperature minus mean surface temperature) as a function of pixel number corresponding to 80 g mass loss.

3. RESULTS AND DISCUSSION

3.1. Evaporative Mass Loss and Moisture Distribution

Figure 2 presents the cumulative evaporation loss curves and the corresponding gravimetric water content profiles for the tested samples. Evaporative water losses were recorded continuously by balances, while the gravimetric water content was determined at the end of the experiments by oven drying (24 h at 105 °C) of samples sectioned layer-by-layer from top to bottom of the sand columns. Each panel includes a reference sample consisting of pure sand saturated with freshwater and three replicates of the test conditions for comparison. It should be noted that the freshwater sample in Figure 2a was tilted for 1 day between days 2 and 4, which further affected the second replication of the 5% NaCl sample (5% NaCl-rep2); both were subsequently adjusted.

The results show that the addition of 5% NaCl significantly reduced cumulative water mass loss compared to freshwater, with a total mass loss approximately 25% lower over the 16-day experiment (Figure 2a). This reduction is consistent with earlier studies, which show that the dissolved salts lower the vapor pressure at the vaporization plane and thereby suppress evaporation.[16,45−47] In addition, precipitation of salt near the surface reduces pore connectivity and permeability, further limiting liquid supply from depth to the surface via capillary pathways.[19,48,49] As a result, NaCl samples retained a higher water content across the profile relative to the freshwater reference sample (Figure 2b). In the absence of shallow water tables, this pattern suggests that formation of salt crusts at the surface may reduce evaporative flux and contribute to moisture preservation within the underlying layers.[15]

In contrast, samples containing 5% PVC saturated with freshwater exhibited enhanced water mass loss, with final cumulative evaporation approximately 20% higher than that of the reference sample and accelerated drying during the first week (Figure 2c). Despite the hydrophobicity of PVC particles, which might restrict capillary transport, our results align with recent studies showing that microplastics smaller than the sand grains can modify soil pore structure and shift the pore-size distribution toward finer pores, thereby extending stage 1 evaporation by sustaining water supply from deeper layers to the surface, where vaporization takes place.[33,35,38,50,51] Gravimetric water content profiles (Figure 2d) further indicate that PVC samples dried more uniformly and did not exhibit a distinct drying front, in contrast to the reference sample, where a noticeable transition separated the dry surface and wetter subsurface layers. This uniformity suggests that PVC increased the tortuosity of liquid pathways and enhanced fluid dispersion, resulting in more homogeneous moisture redistribution during drying.[52−54] Effective capillary behavior is governed not only by pore geometry but also by surface tension and contact angle within pore spaces. In addition to the change in pore structure in the presence of microplastics, local wettability and interfacial processes may change with hydrophobic characteristics of MP particles, thereby altering capillary rise and liquid pathways during evaporative drying.[54]

When PVC and NaCl were combined, the cumulative evaporation (Figure 2e) and water content profiles (Figure 2f) displayed an intermediate behavior. Total mass loss was higher than in NaCl columns but lower than in PVC columns, indicating a competitive interaction. While PVC particles enhance evaporation by structural modification of the pore network, NaCl suppresses it through changing vapor concentration gradients and blocking surface pores. Accordingly, water retention was higher near the surface in comparison with the PVC sample, yet lower at depth relative to the NaCl sample. This highlights that the combined treatment leads to a redistribution pattern reflecting the partial dominance of structural modifications from PVC particles and

https://doi.org/10.1021/acsengineeringau.5c00118
ACS Eng. Au XXXX, XXX, XXX−XXX

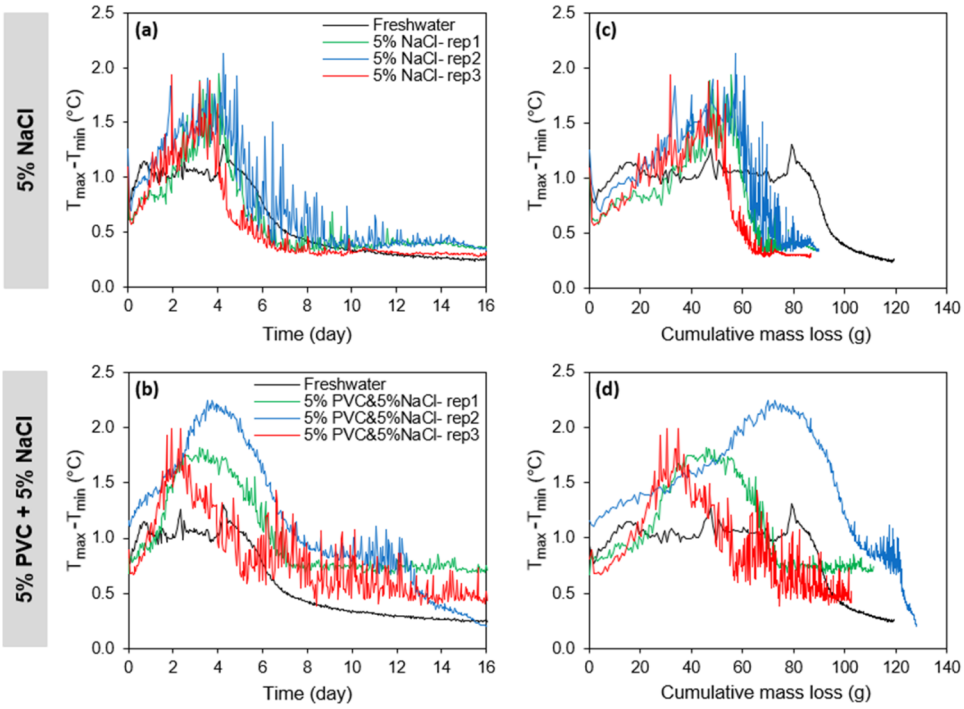

Figure 4. Surface temperature difference ($T_{max} - T_{min}$) as a function of time (a, b), and cumulative mass loss (c, d). The legend refers to the samples saturated with 5% NaCl solution, samples containing 5% PVC saturated with a 5% NaCl solution, and the freshwater sample serving as the reference.

the thermodynamic suppression from the salinity effect and crystallization process.

3.2. Surface Temperature

Surface temperature of the samples was monitored throughout the drying period by using a thermal imager. Figure 3a,b presents the mean surface temperature versus time for each sample. Sand samples saturated with NaCl solution exhibited consistently higher mean surface temperatures than those of the freshwater sample. In addition to the exothermic crystallization process, this further reflects suppressed evaporation due to the formation of salt crusts that may detach from the surface and hinder diffusive vapor fluxes into the air mass.[55,56] In contrast, PVC-NaCl samples showed lower mean surface temperatures relative to NaCl samples, consistent with their higher evaporation rates and the reduced effective thermal conductivity associated with the intrinsically low thermal conductivity of PVC particles.[50]

The evolution of the surface temperature also reflects different stages of evaporation. The surface stays comparatively cool during stage 1 evaporation, which is characterized by capillary flows from the receding drying front to the vaporization plane at the surface. As drying proceeds, the system approaches the onset of stage 2 evaporation, where the vaporization plane recedes into the porous medium and the process shifts from capillary- to diffusion-controlled drying.[3] This transition diminishes latent heat cooling at the surface, leading to a progressive increase in mean surface temperature.[57]

Figure 3c,d displays the surface temperature anomalies (ΔT) at a cumulative mass loss of 80 g. This value was selected as it represents the highest mass-loss level reached by all samples, ensuring a consistent comparison among treatments. ΔT is defined as the deviation of individual pixel temperatures from the mean surface temperature (presented in Figure 3a,b). In NaCl samples, ΔT values decreased and became more spatially uniform, suggesting that the salt crust reduced the local temperature differences by suppressing uneven evaporation and thermal gradients. On the other hand, PVC-NaCl samples exhibited higher ΔT values and more pronounced temperature anomalies. In addition to the impact of microplastics on local evaporation patterns, associated moisture distribution, and reduced effective thermal conductivity, PVC particles likely affected the surface crystallization pattern by preventing the formation of a continuous salt crystal. This combination led to spatially variable evaporative cooling and, consequently, greater surface temperature anomalies. Such fluctuations in surface temperature contribute to microhabitat instability at the soil surface,[58] which can be important for surface-dwelling biota, including biocrusts and microorganisms. For instance, biocrusts strongly respond to coupled temperature-moisture variability, with shifts in their environmental conditions shown to cause large changes in community composition and physiological performance.[59,60] However, further investigation under field conditions incorporating vegetation cover, atmospheric variability, and repeated wetting-drying cycles would help clarify the broader implications of these surface processes.

Figure 4 complements those observations by showing the evolution of the surface temperature difference ($T_{max} - T_{min}$) as a function of time (Figure 4a,4b) and cumulative mass loss (Figure 4c,d) for the freshwater, NaCl, and PVC-NaCl samples. It should be mentioned that T_{max} and T_{min} were defined using the following percentile temperature ranges: T_{max} was calculated as the mean temperature of all pixels above the 90th percentile and T_{min} as the mean temperature of all pixels below the 10th percentile. This procedure minimizes the uncertainty associated with single-pixel extreme values,

https://doi.org/10.1021/acsengineeringau.5c00118
ACS Eng. Au XXXX, XXX, XXX−XXX

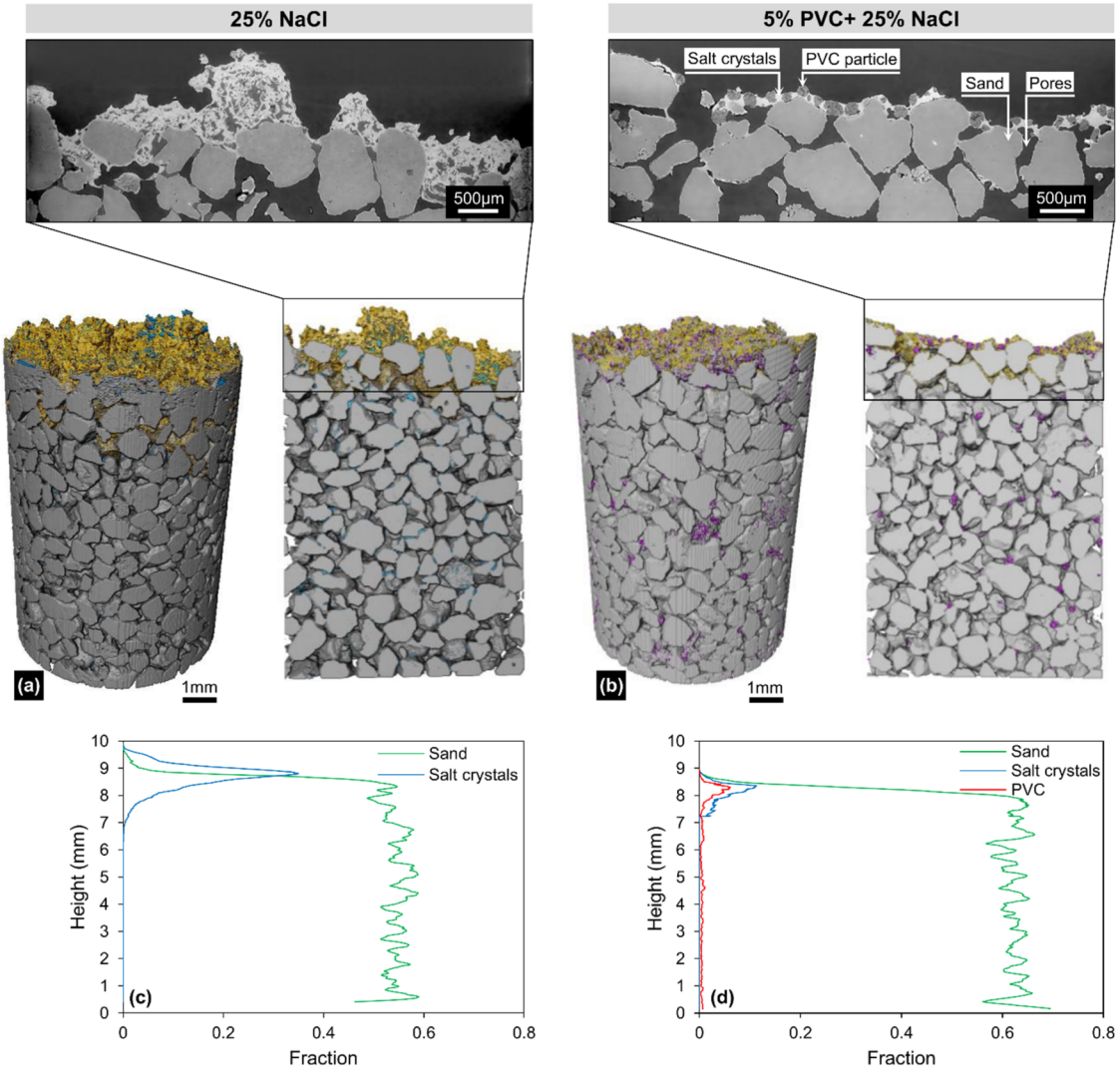

Figure 5. Three-dimensional and cross-sectional μCT images of (a) the sand sample saturated with 25% NaCl and (b) the sample containing 5% PVC saturated with 25% NaCl solution. Fractions shown in gray, yellow, and purple correspond to sand, salt crystals, and PVC particles, respectively. Enlarged views of the samples' top layer are also displayed above the cross-sectional images. (c, d) Component-fraction profiles derived from image analysis for the respective samples.

providing a robust and noise-resistant estimation of the temperature contrast across the sample surfaces.

Across all samples, the temperature difference increased during stage 1 evaporation, where the vaporization plane remains at the surface.[56] It progressively reached a maximum value until the onset of stage 2 evaporation. Eventually, the value of the temperature difference decreased with drying of the surface, marking uniform temperatures over the sample. In NaCl samples, the difference increased sharply during the first 4 days, peaking around 1.8 °C (Figure 4a). Short-term fluctuations reflect rapid salt precipitation and the formation of irregular surface crusts, which enhanced localized evaporative cooling.[12,55,56] In contrast, PVC-saline samples exhibited slightly lower but more sustained values over time (Figure 4b), suggesting that the presence of microplastics resulted in localized moisture and delayed crust formation.

When $T_{max} - T_{min}$ was plotted against cumulative mass loss, NaCl samples reached their peak values at lower mass loss values than the freshwater sample (Figure 4c). Inspection of the optical images at the mass losses corresponding to the peaks shows more extensive surface crystallization in the NaCl samples that reached their peak at a lower mass loss (i.e., sample rep-3). This enhanced crystal formation is consistent with locally reduced vapor pressure and higher ion concentration near the surface, explaining the earlier peak observed in the NaCl samples. Meanwhile, PVC-NaCl samples maintained moderate values across a wider range of mass losses, implying more prolonged and spatially uneven evaporation (Figure 4d).

3.3. Pore-Scale Insights

Pore-scale experiments conducted at DESY provided insights into the spatial distribution of salt crystals and PVC microplastics during the evaporation process. Figure 5a,b presents cross-sectional μCT images of two selected samples, one consisting of pure sand saturated with 25% NaCl and the other composed of sand mixed with 5% PVC (by mass) and saturated with 25% NaCl.

In both samples, salt crystallization occurred at and below the surface. However, a visibly greater accumulation of salt crystals was observed in the pure sand sample, particularly at the top layer, indicating a more extensive upward migration

https://doi.org/10.1021/acsengineeringau.5c00118
ACS Eng. Au XXXX, XXX, XXX−XXX

and surface precipitation of the salt. In contrast, the sample containing PVC exhibited a more irregular distribution of salt, with crystal formation occurring both within the matrix and around the PVC particles, most notably near the surface. The presence of PVC appeared to locally alter the pore structure and nucleation sites, potentially affecting both the pattern and the extent of salt deposition. This observation aligns with previous findings showing that salt crystallization on poorly wetting or heterogeneous surfaces tends to occur at discrete preferential sites, where discontinuous water films control nucleation and growth.[18,61,62] Across these studies, variations in surface energy, wettability, and thin-film stability have been shown to strongly influence the nucleation density, crystal morphology, and spatial mode of crystallization, leading to transitions between efflorescent and subflorescent regimes depending on the degree of wetting and connectivity at the solid−liquid interface. Deposition of the PVC particles was also clearly captured in the cross-sectional view. Microplastics tended to concentrate near the surface, where they became embedded among salt crystals, indicating preferential accumulation zones likely governed by upward capillary-driven flow that transfer PVC particles toward the evaporating surface.[54]

Figure 5c,d shows the component-fraction profiles, derived from image analysis, for sand, salt, and PVC particles in the same samples. These profiles indicate that a higher fraction of salt accumulated near the surface of the pure sand column compared with the sample containing microplastics. This observation supports the hypothesis that salt crystallization is partially inhibited or spatially redistributed in the presence of microplastics, possibly due to changes in capillary connectivity or modifications in the nucleation behavior.

4. SUMMARY AND CONCLUSIONS

We used column-scale evaporation experiments and μCT X-ray imaging to investigate the combined influence of microplastic particles and solution salinity on the water evaporation from porous media and crystallization dynamics. The results show that microplastics and salinity exert distinct and interacting controls on soil evaporation, surface thermal behavior, and salt deposition patterns across scales. Column-scale measurements revealed that NaCl reduced cumulative evaporation, while the addition of PVC increased the total evaporative loss, yielding nearly a 50% difference between drying treatments. These differences were linked to contrasting moisture distribution mechanisms, where NaCl promoted deeper moisture retention and PVC particles caused more uniform water-content profiles by increasing flow tortuosity and enhancing liquid dispersion.

Thermal imaging revealed that these changes were also reflected in the surface temperature behavior. At a drying stage of 80 g mass loss, NaCl samples displayed highly uniform surface temperatures, with ΔT values around 0.5 °C due to suppressed localized evaporation, whereas PVC-NaCl samples showed lower mean surface temperatures but retained spatial temperature variations exceeding 1−1.5 °C, a more than 2-fold increase in thermal heterogeneity. These findings indicate that microplastics reduce mean surface temperatures by enhancing evaporation but substantially increase thermal heterogeneity by influencing the transport of moisture to the surface. Pore-scale μCT imaging confirmed our column-scale observations. Pure sand developed a pronounced and spatially concentrated surface salt crust, whereas PVC redistributed salt over the upper 1−2 mm, yielding irregular crystallization patterns and localized deposition around microplastic particles. Component-fraction profiles further showed higher surface salt fractions in NaCl samples, while PVC reduced and dispersed crystallization by altering the pore geometry and modifying local nucleation sites.

These multiscale observations demonstrated that microplastics can change pore networks, alter coupled water-heat transport processes, and modify crystallization regimes, resulting in distinct evaporation dynamics, shifts in thermal feedbacks, and structural changes at the surface. Quantifying these interactions is essential for understanding how microplastic-contaminated and saline soils regulate soil moisture, surface energy balance, and microhabitat conditions. Future research should investigate a broader diversity of plastic types, soil textures, and field conditions, including their implications for reactive tracer and contaminant transport in porous media, to further expand these findings and inform sustainable land and water management strategies.[63]

AUTHOR INFORMATION

Corresponding Authors

Sahar Jannesarahmadi − *Institute of Geo-Hydroinformatics, Hamburg University of Technology, 21073 Hamburg, Germany; United Nations University Hub on Engineering to Face Climate Change at the Hamburg University of Technology, United Nations University Institute for Water, Environment and Health (UNU-INWEH), 21073 Hamburg, Germany;* orcid.org/0000-0002-2750-9881; Email: sahar.jannesarahmadi@tuhh.de

Milad Aminzadeh − *Institute of Geo-Hydroinformatics, Hamburg University of Technology, 21073 Hamburg, Germany; United Nations University Hub on Engineering to Face Climate Change at the Hamburg University of Technology, United Nations University Institute for Water, Environment and Health (UNU-INWEH), 21073 Hamburg, Germany*; Email: milad.aminzadeh@tuhh.de

Nima Shokri − *Institute of Geo-Hydroinformatics, Hamburg University of Technology, 21073 Hamburg, Germany; United Nations University Hub on Engineering to Face Climate Change at the Hamburg University of Technology, United Nations University Institute for Water, Environment and Health (UNU-INWEH), 21073 Hamburg, Germany;* orcid.org/0000-0001-6799-4888; Email: nima.shokri@tuhh.de

Authors

Birte Hindenlang − *Institute of Metallic Biomaterials, Helmholtz-Zentrum Hereon, 21502 Geesthacht, Germany*

Berit Zeller-Plumhoff − *Institute of Metallic Biomaterials, Helmholtz-Zentrum Hereon, 21502 Geesthacht, Germany; Data-Driven Analysis and Design of Materials, Faculty of Mechanical Engineering and Marine Technologies, University of Rostock, 18059 Rostock, Germany*

Fabian Wilde − *Institute of Materials Physics, Helmholtz-Zentrum Hereon, 21502 Geesthacht, Germany*

Mehdi Mahdaviara − *Department of Earth Sciences, Faculty of Geosciences, Utrecht University, 3584 CB Utrecht, The Netherlands*

Patrick Huber − *United Nations University Hub on Engineering to Face Climate Change at the Hamburg University of Technology, United Nations University Institute for Water, Environment and Health (UNU-INWEH), 21073 Hamburg, Germany; Institute for Materials and X-ray*

https://doi.org/10.1021/acsengineeringau.5c00118
ACS Eng. Au XXXX, XXX, XXX−XXX

Physics, Hamburg University of Technology, 21073 Hamburg, Germany; Centre for X-ray and Nano Science CXNS and Centre for Molecular Water Science CMWS, Deutsches Elektronen-Synchrotron DESY, 22607 Hamburg, Germany; orcid.org/0000-0002-2126-9100

Complete contact information is available at: https://pubs.acs.org/10.1021/acsengineeringau.5c00118

Notes

The authors declare no competing financial interest.

■ ACKNOWLEDGMENTS

We gratefully acknowledge the financial support provided by Deutsche Forschungsgemeinschaft (DFG, German Research Foundation) under grant no. 497539130, and the partial funding from DFG SFB 1313 (project no. 327154368). Support by DFG as part of the Excellence Strategy of the Federal Government and the federal states-EXC 3120/1 BlueMat: Water-Driven Materials (project no. 533771286), is also acknowledged. Funding and resources provided by the Institute of Geo-Hydroinformatics at Hamburg University of Technology and the invaluable technical assistance of Theodor Wassiliou are greatly appreciated. We acknowledge DESY (Hamburg, Germany), a member of the Helmholtz Association HGF, for the provision of experimental facilities. Parts of this research were carried out at PETRA III. Data was collected using the P05 Imaging Beamline operated by Helmholtz-Zentrum Hereon. We would like to thank Jörg Hammel for assistance during the experiments. Beamtime was allocated for proposal I-20230847. Publishing fees supported by the Funding Programme Open Access Publishing of Hamburg University of Technology (TUHH) are acknowledged.

■ REFERENCES

(1) Davarzani, H.; Smits, K.; Tolene, R. M.; Illangasekare, T. Study of the Effect of Wind Speed on Evaporation from Soil through Integrated Modeling of the Atmospheric Boundary Layer and Shallow Subsurface. *Water Resour. Res.* **2014**, *50* (1), 661−680.

(2) Haghighi, E.; Or, D. Evaporation from Wavy Porous Surfaces into Turbulent Airflows. *Transp. Porous Media* **2015**, *110* (2), 225−250.

(3) Or, D.; Lehmann, P.; Shahraeeni, E.; Shokri, N. Advances in Soil Evaporation Physics-A Review. *Vadose Zone J.* **2013**, *12* (4), No. vzj2012.0163.

(4) Shokri, N.; Or, D. What Determines Drying Rates at the Onset of Diffusion Controlled Stage-2 Evaporation from Porous Media? *Water Resour. Res.* 2011; Vol. *47* 9 DOI: 10.1029/2010WR010284.

(5) Aminzadeh, M.; Or, D. Pore-Scale Study of Thermal Fields during Evaporation from Drying Porous Surfaces. *Int. J. Heat Mass Transfer* **2017**, *104*, 1189−1201.

(6) Eloukabi, H.; Sghaier, N.; Ben Nasrallah, S.; Prat, M. Experimental Study of the Effect of Sodium Chloride on Drying of Porous Media: The Crusty−Patchy Efflorescence Transition. *Int. J. Heat Mass Transfer* **2013**, *56* (1−2), 80−93.

(7) Norouzi Rad, M.; Shokri, N.; Sahimi, M. Pore-Scale Dynamics of Salt Precipitation in Drying Porous Media. *Phys. Rev. E* **2013**, *88* (3), No. 032404.

(8) González-Alcaraz, M.; Jiménez-Cárceles, F. J.; Álvarez, Y.; Álvarez-Rogel, J. Gradients of Soil Salinity and Moisture, and Plant Distribution, in a Mediterranean Semiarid Saline Watershed: A Model of Soil-Plant Relationships for Contributing to the Management. *Catena* **2014**, *115*, 150−158.

(9) Dashtian, H.; Wang, H.; Sahimi, M. Nucleation of Salt Crystals in Clay Minerals: Molecular Dynamics Simulation. *J. Phys. Chem. Lett.* **2017**, *8* (14), 3166−3172.

(10) Daliakopoulos, I. N.; Tsanis, I. K.; Koutroulis, A.; Kourgialas, N. N.; Varouchakis, A. E.; Karatzas, G. P.; Ritsema, C. J. The Threat of Soil Salinity: A European Scale Review. *Sci. Total Environ.* **2016**, *573*, 727−739.

(11) Hassani, A.; Azapagic, A.; Shokri, N. Predicting Long-Term Dynamics of Soil Salinity and Sodicity on a Global Scale. *Proc. Natl. Acad. Sci. U.S.A.* **2020**, *117* (52), 33017−33027.

(12) Jannesarahmadi, S.; Aminzadeh, M.; Helmig, R.; Or, D.; Shokri, N. Quantifying Salt Crystallization Impact on Evaporation Dynamics From Porous Surfaces. *Geophys. Res. Lett.* **2024**, *51* (22), No. e2024GL111080.

(13) Licsandru, G.; Noiriel, C.; Geoffroy, S.; Abou-Chakra, A.; Duru, P.; Prat, M. Detachment Mechanism and Reduced Evaporation of an Evaporative NaCl Salt Crust. *Sci. Rep.* **2022**, *12* (1), No. 7473.

(14) Dai, S.; Shin, H.; Santamarina, J. C. Formation and Development of Salt Crusts on Soil Surfaces. *Acta Geotech.* **2016**, *11* (5), 1103−1109.

(15) Nachshon, U.; Weisbrod, N.; Katzir, R.; Nasser, A. NaCl Crust Architecture and Its Impact on Evaporation: Three-Dimensional Insights. *Geophys. Res. Lett.* **2018**, *45* (12), 6100−6108.

(16) Jannesarahmadi, S.; Aminzadeh, M.; Helmig, R.; Or, D.; Oesterle, B.; Shokri, N. The Role of Wind Velocity in Saline Water Evaporation from Porous Media and Surface Salt Crystallization Dynamics. *ACS Earth Space Chem.* **2025**, *9* (7), 1938−1945.

(17) Lasser, J.; Nield, J. M.; Ernst, M.; Karius, V.; Wiggs, G. F. S.; Threadgold, M. R.; Beaume, C.; Goehring, L. Salt Polygons and Porous Media Convection. *Phys. Rev. X* **2023**, *13* (1), No. 011025.

(18) Espinosa-Marzal, R. M.; Scherer, G. W. Mechanisms of Damage by Salt. *Geol. Soc., London Spec. Publ.* **2010**, *331*, 61−77.

(19) Nachshon, U.; Weisbrod, N. Beyond the Salt Crust: On Combined Evaporation and Subflorescent Salt Precipitation in Porous Media. *Transp. Porous Media* **2015**, *110* (2), 295−310.

(20) Shahidzadeh-Bonn, N.; Rafaï, S.; Bonn, D.; Wegdam, G. Salt Crystallization during Evaporation: Impact of Interfacial Properties. *Langmuir* **2008**, *24* (16), 8599−8605.

(21) Nachshon, U.; Weisbrod, N.; Dragila, M. I.; Grader, A.Combined Evaporation and Salt Precipitation in Homogeneous and Heterogeneous Porous Media *Water Resour. Res.* 2011; Vol. *47* 3.

(22) Qazi, M. J.; Salim, H.; Doorman, C. A. W.; Jambon-Puillet, E.; Shahidzadeh, N. Salt Creeping as a Self-Amplifying Crystallization Process. *Sci. Adv.* **2019**, *5* (12), No. eaax1853, DOI: 10.1126/sciadv.aax1853.

(23) Lazhar, R.; Najjari, M.; Prat, M. Combined Wicking and Evaporation of NaCl Solution with Efflorescence Formation: The Efflorescence Exclusion Zone. *Phys. Fluids* **2020**, *32* (6), No. 067106, DOI: 10.1063/5.0007548.

(24) Zou, Y.; Zhang, Y.; Feng, H.; Liu, X.; Guo, J.; Zou, H.; Chen, C.; Huang, S. Occurrence, Fate, and Ecological Impacts of Microplastics in Soil: A Comparative Analysis of Conventional, Biodegradable Microplastics, and Tire Wear Particles. *Environ. Pollut.* **2025**, *386*, No. 127151.

(25) Kang, Q.; Zhang, K.; Dekker, S. C.; Mao, J. Microplastics in Soils: A Comprehensive Review. *Sci. Total Environ.* **2025**, *960*, No. 178298.

(26) Zhong, X.; Qiang, L.; Cheng, J.; Sun, Z.; Hu, H.; Liu, H.; Zhang, R. Aging or Degradation? Transformation Mechanisms of Microplastics in Soil Environments. *Appl. Soil Ecol.* **2025**, *215*, No. 106394.

(27) En-Nejmy, K.; EL Hayany, B.; Al-Alawi, M.; Jemo, M.; Hafidi, M.; El Fels, L. Microplastics in Soil: A Comprehensive Review of Occurrence, Sources, Fate, Analytical Techniques and Potential Impacts. *Ecotoxicol. Environ. Saf.* **2024**, *288*, No. 117332.

(28) Xu, B.; Liu, F.; Cryder, Z.; Huang, D.; Lu, Z.; He, Y.; Wang, H.; Lu, Z.; Brookes, P. C.; Tang, C.; Gan, J.; Xu, J. Microplastics in the Soil Environment: Occurrence, Risks, Interactions and Fate − A Review. *Crit. Rev. Environ. Sci. Technol.* **2020**, *50* (21), 2175−2222.

(29) Grause, G.; Kuniyasu, Y.; Chien, M.-F.; Inoue, C. Separation of Microplastic from Soil by Centrifugation and Its Application to Agricultural Soil. *Chemosphere* **2022**, *288* (P3), No. 132654.

(30) Boots, B.; Russell, C. W.; Green, D. S. Effects of Microplastics in Soil Ecosystems: Above and below Ground. *Environ. Sci. Technol.* **2019**, *53* (19), 11496−11506.
(31) Lin, Z.; Jin, T.; Zou, T.; Xu, L.; Xi, B.; Xu, D.; He, J.; Xiong, L.; Tang, C.; Peng, J.; Zhou, Y.; Fei, J. Current Progress on Plastic/Microplastic Degradation: Fact Influences and Mechanism. *Environ. Pollut.* **2022**, *304*, No. 119159, DOI: 10.1016/j.envpol.2022.119159.
(32) Wan, Y.; Wu, C.; Xue, Q.; Hui, X. Effects of Plastic Contamination on Water Evaporation and Desiccation Cracking in Soil. *Sci. Total Environ.* **2019**, *654*, 576−582.
(33) Jannesarahmadi, S.; Aminzadeh, M.; Raga, R.; Shokri, N. Effects of Microplastics on Evaporation Dynamics in Porous Media. *Chemosphere* **2023**, *311* (P1), No. 137023.
(34) Chy, T. J. Can Microplastic Pollution Change the Water Dynamics of Our Soil Resources?, Ph.D. Thesis; University of Memphis, 2021.
(35) Jiang, X. J.; Liu, W.; Wang, E.; Zhou, T.; Xin, P. Residual Plastic Mulch Fragments Effects on Soil Physical Properties and Water Flow Behavior in the Minqin Oasis, Northwestern China. *Soil Tillage Res.* **2017**, *166*, 100−107.
(36) Guo, Z.; Li, P.; Yang, X.; Wang, Z.; Lu, B.; Chen, W.; Wu, Y.; Li, G.; Zhao, Z.; Liu, G.; Ritsema, C.; Geissen, V.; Xue, S. Soil Texture Is an Important Factor Determining How Microplastics Affect Soil Hydraulic Characteristics. *Environ. Int.* **2022**, *165*, No. 107293.
(37) Feng, H.; Xing, X.; Du, J.; Jiao, S.; Yu, M.; Wang, W. Concentration- and Size-Dependent Influences of Microplastics on Soil Hydraulic Properties and Water Flow. *Eur. J. Soil Sci.* **2025**, *76* (1), No. e70049, DOI: 10.1111/ejss.70049.
(38) Wang, Z.; Li, W.; Li, W.; Yang, W.; Jing, S. Effects of Microplastics on the Water Characteristic Curve of Soils with Different Textures. *Chemosphere* **2023**, *317*, No. 137762.
(39) Fuller, S.; Gautam, A. A Procedure for Measuring Microplastics Using Pressurized Fluid Extraction. *Environ. Sci. Technol.* **2016**, *50* (11), 5774−5780.
(40) Moosmann, J.; Ershov, A.; Weinhardt, V.; Baumbach, T.; Prasad, M. S.; LaBonne, C.; Xiao, X.; Kashef, J.; Hofmann, R. Time-Lapse X-Ray Phase-Contrast Microtomography for in Vivo Imaging and Analysis of Morphogenesis. *Nat. Protoc.* **2014**, *9* (2), 294−304.
(41) Moosmann, J. Moosmann/Matlab **2021** DOI: 10.5281/zenodo.5118737. (accessed November 20, 2025−11−20).
(42) van Aarle, W.; Palenstijn, W. J.; De Beenhouwer, J.; Altantzis, T.; Bals, S.; Batenburg, K. J.; Sijbers, J. The ASTRA Toolbox: A Platform for Advanced Algorithm Development in Electron Tomography. *Ultramicroscopy* **2015**, *157* (2015), 35−47.
(43) Bruns, S.; Stipp, S. L. S.; Sørensen, H. O. Looking for the Signal: A Guide to Iterative Noise and Artefact Removal in X-Ray Tomographic Reconstructions of Porous Geomaterials. *Adv. Water Resour.* **2017**, *105*, 96−107.
(44) Schindelin, J.; Arganda-Carreras, I.; Frise, E.; Kaynig, V.; Longair, M.; Pietzsch, T.; Preibisch, S.; Rueden, C.; Saalfeld, S.; Schmid, B.; Tinevez, J.-Y.; White, D. J.; Hartenstein, V.; Eliceiri, K.; Tomancak, P.; Cardona, A. Fiji: An Open-Source Platform for Biological-Image Analysis. *Nat. Methods* **2012**, *9* (7), 676−682.
(45) Norouzi Rad, M.; Shokri, N.Nonlinear Effects of Salt Concentrations on Evaporation from Porous Media *Geophys. Res. Lett.* 2012; Vol. *39* 4.
(46) Shokri-Kuehni, S. M. S.; Rad, M. N.; Webb, C.; Shokri, N. Impact of Type of Salt and Ambient Conditions on Saline Water Evaporation from Porous Media. *Adv. Water Resour.* **2017**, *105*, 154−161.
(47) Sghaier, N.; Prat, M. Effect of Efflorescence Formation on Drying Kinetics of Porous Media. *Transp. Porous Media* **2009**, *80* (3), 441−454.
(48) Mercury, L.; Tas, N.; Zilberbrand, M. *Transport and Reactivity of Solutions in Confined Hydrosystems*; Springer, 2013.
(49) Jambhekar, V. A.; Helmig, R.; Schröder, N.; Shokri, N. Free-Flow−Porous-Media Coupling for Evaporation-Driven Transport and Precipitation of Salt in Soil. *Transp. Porous Media* **2015**, *110* (2), 251−280.
(50) Aminzadeh, M.; Kokate, T.; Shokri, N. Microplastics in Sandy Soils: Alterations in Thermal Conductivity, Surface Albedo, and Temperature. *Environ. Pollut.* **2025**, *372*, No. 125956.
(51) Maillet, B.; Dittrich, G.; Huber, P.; Coussot, P. Diffusionlike Drying of a Nanoporous Solid as Revealed by Magnetic Resonance Imaging. *Phys. Rev. Appl.* **2022**, *18* (5), No. 054027.
(52) Aminzadeh, M.; Kokate, T.; Chaudhry, A. U.; Rabbani, H.; Bijeljic, B.; Blunt, M. J.; Shokri, N. Microplastic-Induced Alterations in Water Flow and Solute Transport Dynamics in Soil. *Sci. Rep.* **2025**, *15* (1), No. 42941.
(53) Sahimi, M.; Hughes, B. D.; Scriven, L. E.; Ted Davis, H. Dispersion in Flow through Porous Media—I. One-Phase Flow. *Chem. Eng. Sci.* **1986**, *41* (8), 2103−2122.
(54) Cramer, A.; Benard, P.; Zarebanadkouki, M.; Kaestner, A.; Carminati, A. Microplastic Induces Soil Water Repellency and Limits Capillary Flow. *Vadose Zone J.* **2023**, *22* (1), No. e20215.
(55) Misyura, S. Y. Evaporation and Heat Transfer of Aqueous Salt Solutions during Crystallization. *Appl. Therm. Eng.* **2018**, *139*, 203−212.
(56) Shokri-Kuehni, S. M. S.; Vetter, T.; Webb, C.; Shokri, N. New Insights into Saline Water Evaporation from Porous Media: Complex Interaction between Evaporation Rates, Precipitation, and Surface Temperature. *Geophys. Res. Lett.* **2017**, *44* (11), 5504−5510.
(57) Aminzadeh, M.; Or, D. Temperature Dynamics during Nonisothermal Evaporation from Drying Porous Surfaces. *Water Resour. Res.* **2013**, *49* (11), 7339−7349.
(58) Harte, J.; Torn, M. S.; Chang, F.-R.; Feifarek, B.; Kinzig, A. P.; Shaw, R.; Shen, K. Global Warming and Soil Microclimate: Results from a Meadow-Warming Experiment. *Ecol. Appl.* **1995**, *5* (1), 132−150.
(59) Johnson, S. L.; Kuske, C. R.; Carney, T. D.; Housman, D. C.; Gallegos-Graves, L. V.; Belnap, J. Increased Temperature and Altered Summer Precipitation Have Differential Effects on Biological Soil Crusts in a Dryland Ecosystem. *Global Change Biol.* **2012**, *18* (8), 2583−2593.
(60) Zelikova, T. J.; Housman, D. C.; Grote, E. E.; Neher, D. A.; Belnap, J. Warming and Increased Precipitation Frequency on the Colorado Plateau: Implications for Biological Soil Crusts and Soil Processes. *Plant Soil* **2012**, *355* (1−2), 265−282.
(61) Veran-Tissoires, S.; Marcoux, M.; Prat, M. Discrete Salt Crystallization at the Surface of a Porous Medium. *Phys. Rev. Lett.* **2012**, *108* (5), No. 054502.
(62) Osman, A.; Leaper, S.; Sreepal, V.; Gorgojo, P.; Stitt, H.; Shokri, N. Dynamics of Salt Precipitation on Graphene Oxide Membranes. *Cryst. Growth Des.* **2019**, *19* (1), 498−505.
(63) Akanji, L. T.; Falade, G. K. Closed-Form Solution of Radial Transport of Tracers in Porous Media Influenced by Linear Drift. *Energies* **2019**, *12* (1), No. 29.

https://doi.org/10.1021/acsengineeringau.5c00118
ACS Eng. Au XXXX, XXX, XXX−XXX